IJMOT

INTERNATIONAL JOURNAL OF MICROWAVE AND OPTICAL TECHNOLOGY

VOL. 1, NO. 1, JUNE 2006

UWB Monopole Antenna with a Top-hat Sleeve

Wei Qiao[1], *Zhi Ning Chen[2], and Ke Wu[3]

[1]Department of Electric and Computer Engineering
Georgia Institute of Technology
Atlanta, Georgia 30332, USA

[2]Department of Radio Systems
Institute for Infocomm Research
20 Science Park Road, #02-21/25 TeleTech Park, Singapore 119260
Fax: (65)6779 5441 ; Tel : (65) 6870 9161; E-mail: chenzn@i2r.a-star.edu.sg

[3]Department of Electrical & Computer Engineering
ECOLE Polytechnique Montreal
P. O. Box 6079, Station Centre-ville, Montreal Quebec, Canada H3C 3A7

***Abstract*— This paper presents a top-hat sleeve monopole antenna for ultra-wideband (UWB) applications. The proposed antenna comprises a stem, a dielectric coat, and a top hat sleeve. A modal expansion technique used in cylindrical coordinate system is applied to study the impedance and radiation characteristics of the antenna. Influences of varying parameters of the antenna on impedance matching and radiation patterns are examined. The design demonstrates an extraordinarily broad bandwidth of up to 105% (2.65-7.95GHz), which covers the lower UWB band of 3.1-4.8 GHz very well and quite stable radiation performances across the bandwidth.**

***Index Terms*— Ultra-wideband antennas, sleeve monopoles, modal expansion methods, radiation patterns**

I. INTRODUCTION

The coaxially fed monopoles, holding the feature of geometrical simplicity, cost effectiveness and modal purity, are attractive to various microwave devices and communication systems. Many efforts have long been devoted to further enhance their impedance and radiation bandwidths. For example, a biconical antenna was used with the idea from a tapered transmission line or electromagnetic horn. Later, finite cones were taken into account and used in practical designs for the VHF and UHF frequency ranges. After that, one of the above-mentioned cones mounted on an infinitely ground plane formed monopoles or unipoles [1]. As geometrical approximations to solid conical or monopole antennas, bow-tie and triangular sheet antennas as well as wire-constructed bow-tie antennas were employed to approximate conical body-of-revolution antennas [2-4]. A thick dipole or monopole can be considered to be a special form of the conical antenna with a cone angle of zero [5]. As variations of cones and dipoles, conical skirt monopole and discone antennas feature broadband characteristics discussed in [6]. Basically, such antennas are linear monopoles with vertical polarization and omni-directional radiation patterns. Recently, planar monopoles have been widely investigated, where the planar radiators are used for ultra-wideband (UWB) systems [7-10]. Helical antennas are the monopoles operating in a normal or an axial mode with broadened bandwidth [11]. In addition, a variety of loaded monopole antennas also have shown their broadband characteristics [12]. Loading elements may be passive or active, distributed or lumped, lossy or lossless medium, dielectric or metallic and so on.

On the other hand, using an outer sleeve, namely the extension of a coaxial line, the feed point at the bottom of the monopole is moved upward from the ground plane to the center of the monopole so that the radiation performance of the broadband monopole can be improved due to in-

phase induced currents on the sleeve and monopole within a large frequency range [13, 14].

In this paper, a monopole antenna with a top-hat sleeve is proposed for UWB applications. A modal expansion technique is extended to model and design the monopole antenna [12, 15-17]. Moreover, parametric study is carried out to examine the bandwidth and matching factor (MF) defined in [15]. The proposed antenna is to be applied to UWB applications by achieving broad impedance bandwidth covering the lower UWB band of 3.1-4.8 GHz [18].

II. FORMULATION

The geometry of the proposed antenna is described in Fig. 1 with a circular cylindrical coordinates (ρ, ϕ, z) in which the vertical z-axis is centered through the monopole connected to the coaxial line. A modal expansion technique is used to model the proposed antenna radiating into a half space over a ground plane [12, 15-17]. In this method, a fictitious ground plane caps the antenna at a distance p so that the electric and magnetic field components in the region between two ground planes can be formulated in terms of cylindrical harmonic expansions. The existence of the fictitious upper ground plane hardly affects numerical solutions when $p - h > \lambda_0$ [12].

First, the region between two ground planes is divided into six subregions, which are marked by permittivity ε_n (=$\varepsilon_0\varepsilon_{rn}$, n=1, …,6) and permeability μ_0. A source region with gap d, uniform electric field and a phasor voltage source V_0 is designated to drive the antenna stem. Next, electric and magnetic fields in the subregions are formulated by an electric type (TM^z) Hertz potential [19]. After that, the expansion coefficients are determined by the enforcement of boundary and continuity conditions at the interfaces of subregions by a Fourier least-square integration. Subsequently, the fields in the subregions and the induced currents on the stem are obtained. Finally, the impedance matching and radiated fields are evaluated.

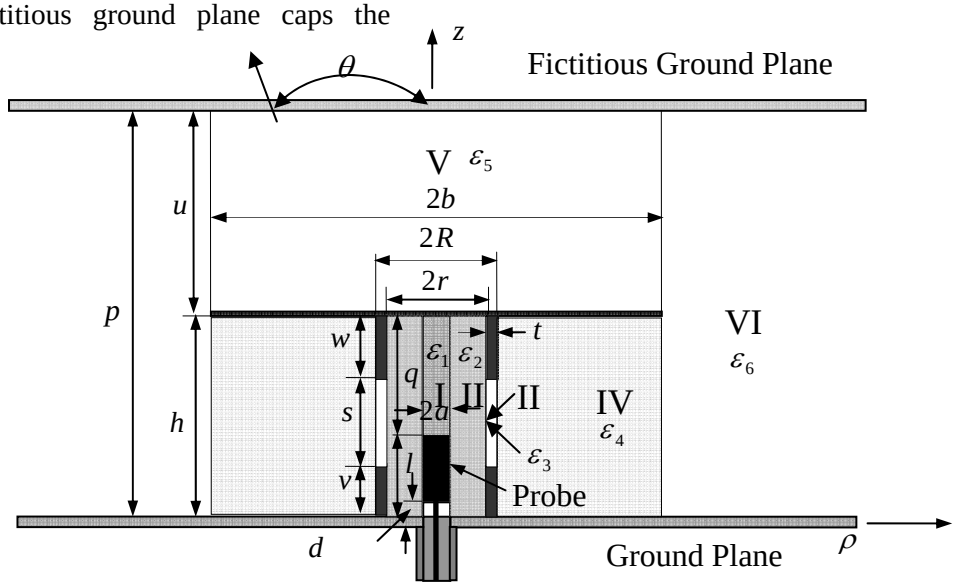

Fig. 1. Geometrical description and physical notation of the proposed dielectric-loaded top-hat monopole with double sleeves between two ground planes

Enforcement of the PEC conditions on both ground planes, the top-hat, the top of the stem, and the ends of the two sleeves yields truncated eigenmode expansions for nonzero field components in the z-coordinate. For example,

the field formulations in subregion II (dielectric jacket) with $a \le \rho \le r$ and $0 \le z \le h$ are given by

$$E_z^{II}(\rho, z) = \frac{1}{j\omega\varepsilon_{r2}\varepsilon_0}\sum_{n=0}^{N_2} k_{\rho 2n}^2 [a_{2n} J_0(k_{\rho 2n}\rho) + b_{2n} N_0(k_{\rho 2n}\rho)]\cos\left(\frac{n\pi}{h} z\right) \quad (1a)$$

$$H_\phi^{II}(\rho, z) = \sum_{n=0}^{N_2} k_{\rho 2n} [a_{2n} J_1(k_{\rho 2n}\rho) + b_{2n} N_1(k_{\rho 2n}\rho)]\cos\left(\frac{n\pi}{h} z\right) \quad (1b)$$

with $k_2^{\,2} = \varepsilon_{r2} k_0^{\,2}$, and

$$k_{\rho 2n} = \pm\sqrt{k_2^2 - (n\pi/h)^2} = \begin{cases} \sqrt{k_2^2 - (n\pi/h)^2} & k_2 \ge (n\pi/h) \\ -j\sqrt{(n\pi/h)^2 - k_2^2} & k_2 \le (n\pi/h) \end{cases}$$

Similarly, the field formulations in subregion IV with $R \le \rho \le b, 0 \le z \le h$ is

$$E_z^{IV}(\rho, z) = \frac{1}{j\omega\varepsilon_{r4}\varepsilon_0}\sum_{n=0}^{N_4} k_{\rho 4n}^2 [a_{4n} H_0^{\,(1)}(k_{\rho 4n}\rho) + b_{4n} H_0^{\,(2)}(k_{\rho 4n}\rho)]\cos\left(\frac{n\pi}{h} z\right) \quad (2a)$$

$$H_\phi^{IV}(\rho, z) = \sum_{n=0}^{N_4} k_{\rho 4n} [a_{4n} H_1^{\,(1)}(k_{\rho 4n}\rho) + b_{4n} H_1^{\,(2)}(k_{\rho 4n}\rho)]\cos\left(\frac{n\pi}{h} z\right) \quad (2b)$$

with $k_4^{\,2} = \varepsilon_{r4} k_0^{\,2}$, and

$$k_{\rho 4n} = \pm\sqrt{k_4^2 - (n\pi/h)^2} = \begin{cases} \sqrt{k_4^2 - (n\pi/h)^2} & k_4 \ge (n\pi/h) \\ -j\sqrt{(n\pi/h)^2 - k_4^2} & k_4 \le (n\pi/h) \end{cases}$$

The field formulations in subregion V ($0 \le \rho \le b, h \le z \le p$) above the top hat:

$$E_z^V(\rho, z) = \frac{1}{j\omega\varepsilon_{r5}\varepsilon_0}\sum_{n=0}^{N_5} a_{5n} k_{\rho 5n}^2 J_0(k_{\rho 5n}\rho)\cos\left(\frac{n\pi}{u}(z-h)\right) \quad (3a)$$

$$H_\phi^V(\rho, z) = \sum_{n=0}^{N_5} a_{5n} k_{\rho 5n} J_1(k_{\rho 5n}\rho)\cos\left(\frac{n\pi}{u}(z-h)\right) \quad (3b)$$

with $k_5^{\,2} = \varepsilon_{r5} k_0^{\,2}$, and

$$k_{\rho 5n} = \pm\sqrt{k_5^2 - (n\pi/u)^2} = \begin{cases} \sqrt{k_5^2 - (n\pi/u)^2} & k_5 \ge (n\pi/u) \\ -j\sqrt{(n\pi/u)^2 - k_5^2} & k_5 \le (n\pi/u) \end{cases}$$

In the above equations, $J_m(\cdot)$, $N_m(\cdot)$, $H_m^{(1)}(\cdot)$ and $H_m^{(2)}(\cdot)$ are, respectively, Bessel functions of the first and the second kind, and Hankel functions of the first and the second kind, having the order $m = 0$ or 1. Similarly, the field components in other subregions can be formulated in terms of Bessel and Hankel functions.

The application of remaining boundary and continuity conditions on the tangential fields

determines the expansion coefficients by using Fourier least-square integration over the boundaries and interfaces of the subregions. Combination of the linear equations derived from this procedure leads to a complex matrix equation system (4) of the order $N_t = 2N_2 + 2N_3 + 2N_4 + N_5 + 7$, which is set up for calculation of the expansion coefficients a_{2n}, b_{2n}, a_{3n}, b_{3n}, a_{4n}, b_{4n} and a_{5n}.

$$\begin{bmatrix} [Z_{11}] & [Z_{12}] & [0_{13}] & [0_{14}] & [0_{15}] & [0_{16}] & [0_{17}] \\ [Z_{21}] & [Z_{22}] & [Z_{23}] & [Z_{24}] & [0_{25}] & [0_{26}] & [0_{27}] \\ [Z_{31}] & [Z_{32}] & [Z_{33}] & [Z_{34}] & [0_{35}] & [0_{36}] & [0_{37}] \\ [0_{41}] & [0_{42}] & [Z_{43}] & [Z_{44}] & [Z_{45}] & [Z_{46}] & [0_{47}] \\ [0_{51}] & [0_{52}] & [Z_{53}] & [Z_{54}] & [Z_{55}] & [Z_{56}] & [0_{57}] \\ [0_{61}] & [0_{62}] & [0_{63}] & [0_{64}] & [Z_{65}] & [Z_{66}] & [Z_{67}] \\ [0_{71}] & [0_{72}] & [0_{73}] & [0_{74}] & [Z_{75}] & [Z_{76}] & [Z_{77}] \end{bmatrix} \times \begin{bmatrix} [a_2] \\ [b_2] \\ [a_3] \\ [b_3] \\ [a_4] \\ [b_4] \\ [a_5] \end{bmatrix} = \begin{bmatrix} [V_1] \\ [0_2] \\ [0_3] \\ [0_4] \\ [0_5] \\ [0_6] \\ [0_7] \end{bmatrix} \tag{4}$$

Once the expansion coefficients are obtained, the induced current on the monopole can be calculated by

$$I(z) = 2\pi a H_\phi^{II}(a,z) = 2\pi a \sum_{n=0}^{N_2} k_{\rho 2n}[a_{2n} J_1(k_{\rho 2n} a) + b_{2n} N_1(k_{\rho 2n} a)] \cos\left(\frac{n\pi}{h} z\right) \tag{5}$$

Then the input impedance can be easily evaluated by using $Z_{in} = V_0 / I(0)$ with $I(0)$ attained from (5).

The far-zone radiated fields are evaluated by using Green's function integration over the outer surface of the imaged top-hat dipole. As shown in Fig. 1, there are three different current contributions to this integration: (1) physical electric currents on the outer surfaces of the top and bottom PEC hat ($z=h$, and $0 \le \rho \le b$); (2) equivalent electric currents, $J_z(z) = H_\phi^{IV}(b,z)$, over the interface of region III and IV ($\rho = b$, and $-h \le z \le h$), and (3) equivalent magnetic current, $M_\phi(z) = E_z^{IV}(b,z)$ over this same surface.

The θ -directed electric field component $E_\theta^1(r,\theta)$ in the far-zone due to the physical electric currents on the outer surfaces of the top and bottom PEC hat is:

$$rE_\theta^1(r,\theta) = -j\omega\mu_0 \cos\theta \sin(k_0 h \cos\theta) e^{jk_0 r} \sum_{n=0}^{N_5} a_{5n} I_n^1 \tag{6}$$

where, the integral within the sum can be evaluated as

$$\begin{aligned} I_n^1 &= \int_0^b k_{\rho 5n} \rho J_1(k_{\rho 5n}\rho) J_1(k_0 \rho \sin\theta) d\rho \\ &= \frac{k_{\rho 5n} b}{k_{\rho 5n}^2 - k_0^2 \sin^2\theta} \left[k_0 \sin\theta J_1(k_{\rho 5n} b) J_0(k_0 b \sin\theta) - k_{\rho 5n} J_0(k_{\rho 5n} b) J_1(k_0 b \sin\theta) \right] \end{aligned} \tag{7}$$

Next, we calculate the radiated field contribution $E_\theta^2(r,\theta)$ from the equivalent electric current, $J_z(z) = H_\phi^{IV}(b,z)$ on the outside cylindrical surface of the imaged dipole.

$$rE_\theta^2(r,\theta) = j\omega\mu_0 b\sin\theta J_0(k_0 b\sin\theta)e^{jk_0 r}\sum_{n=0}^{N_4} k_{\rho 4n}[a_{4n}H_1^{(1)}(k_{\rho 4n}b)+b_{4n}H_1^{(2)}(k_{\rho 4n}b)]I_n^2 \quad (8)$$

where

$$I_n^2 = \int_0^h \cos\left(\frac{n\pi}{h}z\right)\cos(k_0 z\cos\theta)dz = (-1)^n \sin(k_0 h\cos\theta)\frac{k_0\cos\theta}{k_0^2\cos^2\theta-(\frac{n\pi}{h})^2} \quad (9)$$

The radiated electric field component $E_\theta^3(r,\theta)$ generated by the equivalent magnetic current $M_\phi(z) = E_z^{IV}(b,z)$ on the outside cylindrical surface of the imaged dipole is:

$$rE_\theta^3(r,\theta) = -j\eta_0 b J_1(k_0 b\sin\theta)\frac{1}{\varepsilon_{r4}}e^{jk_0 r}\sum_{n=0}^{N_4} k_{\rho 4n}^2[a_{4n}H_1^{(1)}(k_{\rho 4n}b)+b_{4n}H_1^{(2)}(k_{\rho 4n}b)]I_n^2 \quad (10)$$

Finally, the total far-zone radiated field pattern $|rE_\theta|$ can be evaluated by

$$|rE_\theta| = |rE_\theta^1 + rE_\theta^2 + rE_\theta^3| \quad (11)$$

III. RESULTS AND DISCUSSION

Based on the modal expansion formulation, the monopole is optimized for a UWB bandwidth. The referenced dimensions are given in Table I. With numerical experiments, the computational convergence and determine the number of expansion modes were assesses and N_1=40, N_2=55, N_3=40, N_4=30, and N_5=80 are adopted.

First, one simple monopoles ($w\rightarrow 0$, $v\rightarrow 0$, ε_{r2}=1.0, h=3.1λ_0) and p=6.97λ_0) and one sleeve monopole ($w\rightarrow 0$, v =0.45λ_0, l=0.7λ_0, ε_{r2}=1.0, h=3.1λ_0, p=6.97λ_0) are exemplified and compared with the experimental results given in [16] and [17]. Then, the antenna with dimensions listed in Table I is optimized for broad impedance bandwidth as shown in Fig. 2(a) and 2(b). It is seen that the input resistance curve with a double-hump shape and small input reactance near zero in the frequency range 2.5-8.5 GHz. Two new parasitic modes due to the sleeve and the top-hat are excited well and appeared close to the operating mode generated by a simple monopole as shown in Fig. 2(b). The achieved impedance bandwidth for VSWR≤2:1 is 100% with a frequency range of 2.65-7.95 GHz. To further validate the results, a commercial EM simulator IE3D was used as shown in Fig. 2(c) and 2(d).

The Fig. 3 shows the effects of varying top-hat heights on the input impedance, where other dimensions are fixed. The results show that the top-hat height has a significant influence on the lower resonance. The peak value of input resistance at the lower hump increases and shifts rightwards as the height w is extended, while the input reactance reaches its minimum peak value and keeps center when the height w is around 12.41 mm.

Fig. 4 exhibits the significant effects of varying bottom sleeve length on the input impedance response. As shown in Fig. 4(a), the frequency of the higher series resonance (around 6 GHz) decreases from 6 to 5 GHz as the length v increases from 6.8 to 7.8 mm.

TABLE I DIMENSIONS OF THE PROPOSED ANTENNA (UNIT: mm)

l	h	v	w	a	d	r	t	b	$\varepsilon_{rn}(n=1,3,\cdots,5)$	ε_{r2}
20.51	45.0	7.30	12.41	0.635	5.0a	4.7574	0.28	15.50	1.0	2.01

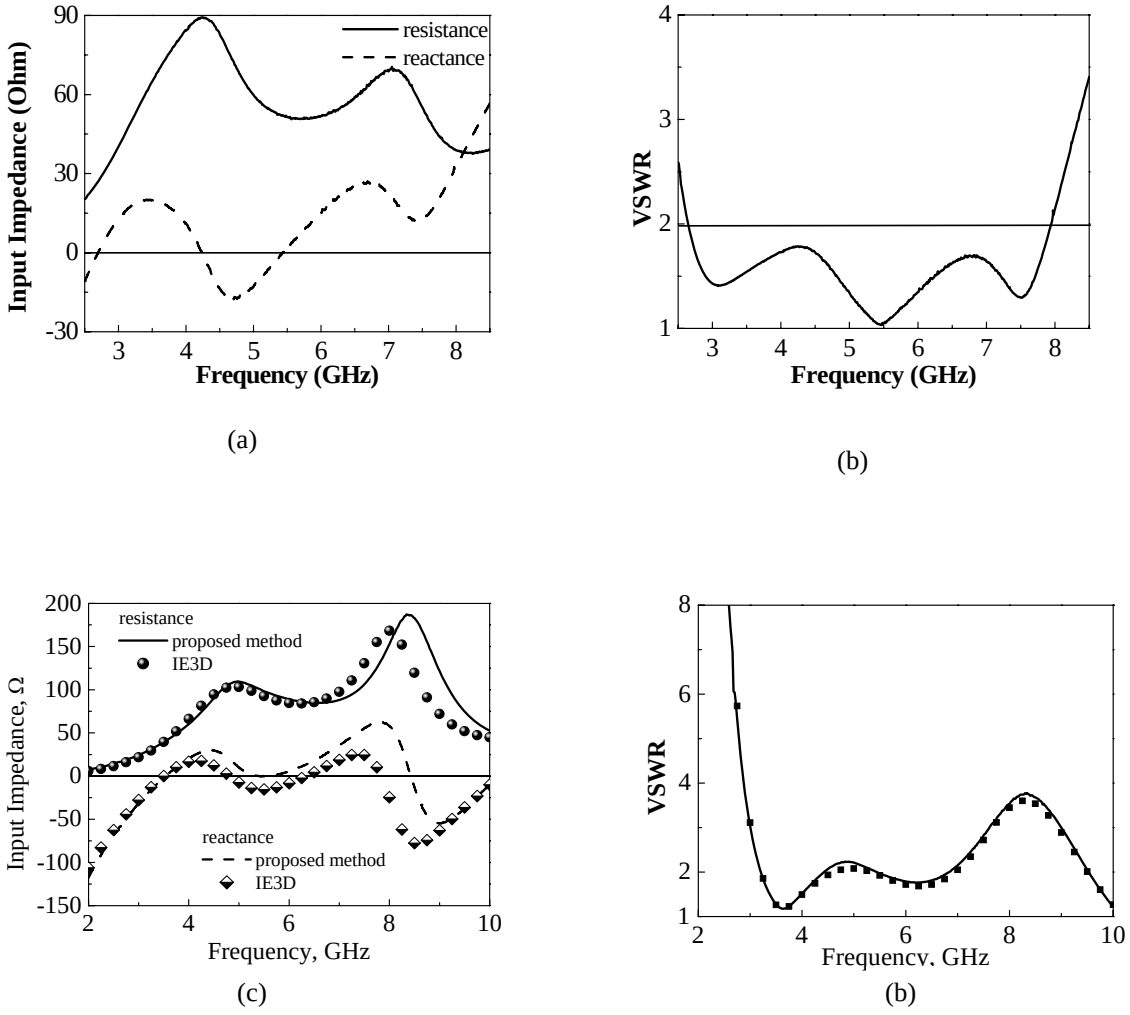

Fig. 2. Calculated frequency responses of proposed antenna (a) input impedance and (b) VSWR as well as the comparison of two methods: (c) input impedance and (d) VSWR

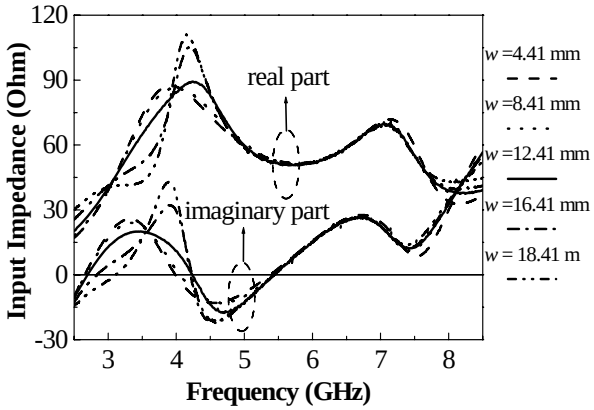

Fig. 3. Calculated input impedance of proposed antenna for varying top-hat heights *w*

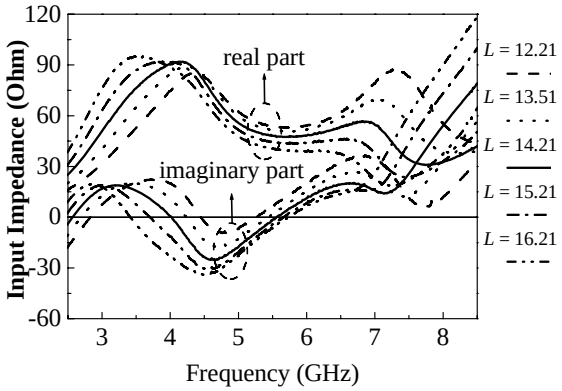

Fig. 5. Calculated input impedance for varying stem lengths *L*

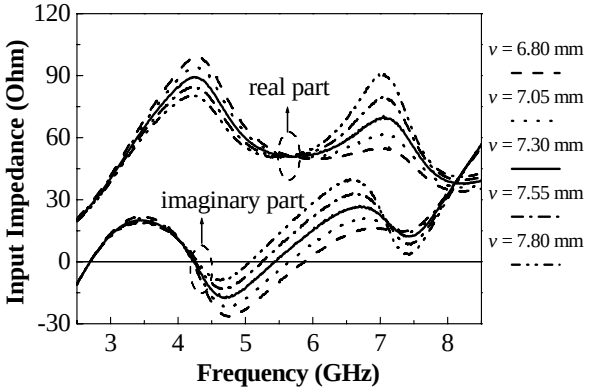

Fig. 4. Calculated input impedance of proposed monopole for varying sleeve lengths *v*

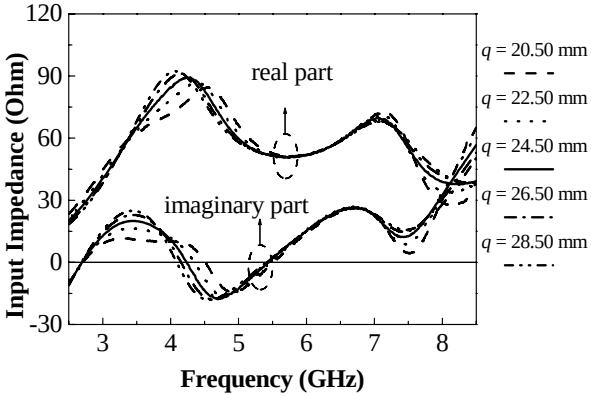

Fig. 6. Calculated input impedance for varying spacing *q*

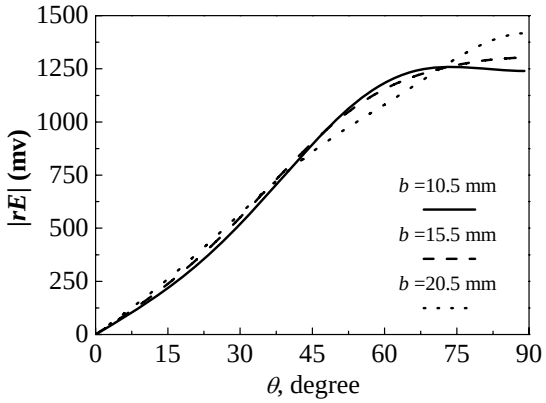

Fig. 7. Radiated field patterns for varying top-hat radii *b* at 5.5GHz

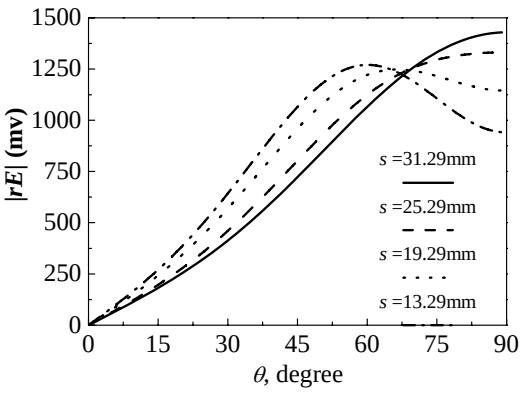

Fig. 8. Radiated patterns for varying aperture lengths *s* by changing top-hat heights *w* at 5.5GHz

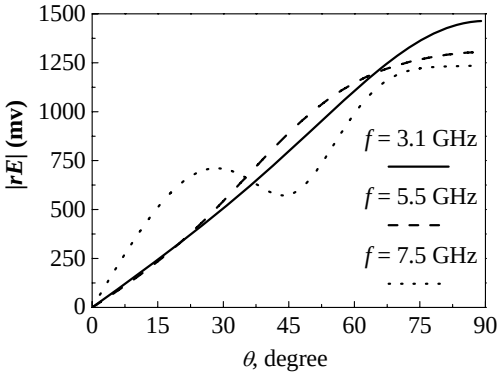

Fig. 9 Radiated patterns at 3.1, 5.5, and 7.5GHz

Moreover, the length of the stem $L= l\text{-}v$ significantly affects the input impedance characteristics as shown in Fig. 5. Decreasing the length L pushes the value of second peak resistance and reactance, and the second resonance frequency up. This degrades the impedance matching. The coupling between the loading and the monopole depends on the length L, especially as the lengths v, w, and spacing h are fixed.

The impedance response for varying spacing q is shown in Fig. 6. Different from the structure discussed in [16] and [17] integrated into the parallel-plate waveguide, the spacing q has a slight influence on the impedance, in particular on the higher resonance due to a finite-diameter top-hat. Another difference is that the top-hat height w has a trivial effect on the higher resonance as well.

The far-region radiated field patterns at 5.5 GHz are examined and shown in Fig. 7 where the top-hat radii b varies. Clearly, the radiation patterns show the same features as that of a conventional simple monopole antenna and are slightly affected by varying top-hat radius b whereas Fig. 8 shows the significant impact of varying aperture length s on the far-region radiated field patterns, where the antenna has a small top-hat radius b = 5.50 mm and operates at 5.5 GHz. It suggests that as the aperture length decreasing from 31.29 to 13.29 mm, the maximum radiation direction moves off the horizon from $\theta = 90^o$ to 55^o. This directly attributes to the change in the distribution of currents on outside surface of the antennas because the modes within the aperture have varied greatly.

Furthermore, the radiation patterns within the bandwidth are examined at three typical frequencies, 3.1, 5.5, and 7.5 GHz. Fig. 9 suggests that due to the sleeves the radiation characteristics hardly change. Thus, this design is capable of providing the quite broad bandwidths for both impedance and radiation patterns.

IV. DESIGN CONSIDERATIONS

For design purpose, the effects of varying structural parameters on the bandwidth and matching condition of the antenna are discussed.

In practical, the enough bandwidth and good matching are always attractive to antenna designers. As done in [16, 17], the matching factor is used to assess the matching feature. As the parameter VSWR is used to describe the matching, the MF is defined as

$$MF_{VSWR\le 2.0} = \frac{\Delta A_{VSWR\le 2.0}}{\Delta f_{VSWR\le 2.0}} \qquad (12)$$

where $\Delta A_{VSWR\leq 2}$ denotes the area surrounded by the VSWR≤2.0 curve and the VSWR≤2.0 line, and $\Delta f_{VSWR\leq 2}$ is the frequency range in which VSWR≤2.0 is always satisfied. The term (2.0-$MF_{VSWR\leq 2}$) represents the average VSWR value in the frequency range for VSWR≤2.0. The average VSWR, for instance, is 1.436 as the MF is 0.564 for q = 20.5 mm, and the average VSWR is 1.537 as the MF is 0.463 for q = 30.5 mm. Clearly, the matching condition for q = 20.5mm is better than that for q = 30.5 mm therefore higher matching factor means better matching condition. In this way, the parameter MF gives a simple and direct approach to assess the critical matching characteristics of the antenna.

Fig. 10 shows that the matching condition for L = 13.21 mm is better than that for L = 15.21 mm, q<22.5 although the bandwidths are almost the same. Therefore, a design tradeoff should be considered based on systems requirements in terms of geometrical size, impedance bandwidth, and matching condition. For example, Fig. 10 suggests that the bandwidth and matching behavior for L = 13.21 mm are better than those for L = 11.21 and 15.21 mm.

The typical bandwidths and MF behavior for varying stem length L are shown in Fig. 11. Both bandwidth and MF curves suggest that the better behavior for shorter spacing. Furthermore, optimal matching and bandwidth are in the range of L = 13.0-14.5 mm.

Fig. 12 compares the bandwidth and MF with respect to the top-hat height w for varying stem lengths L = 11.21, 13.21, and 15.21 mm. The bandwidths reach their maxima in the range of w = 10.0-14.5 mm. However, the MF curves show that the matching behaviors are not so good for the maximum bandwidths.

Last, the effects of varying sleeve length v on the bandwidth and matching condition are taken into account. Fig. 13 shows that the bandwidth is more sensitive to the bottom sleeve length than the matching behavior in a wide range of w = 6.30-8.80 mm.

In addition, the investigation shows that the thickness, t has slightly affects the performance of the antenna when it varies from 0.18 to 0.38 mm but the dielectric constant of the dielectric loading greatly affects the impedance matching.

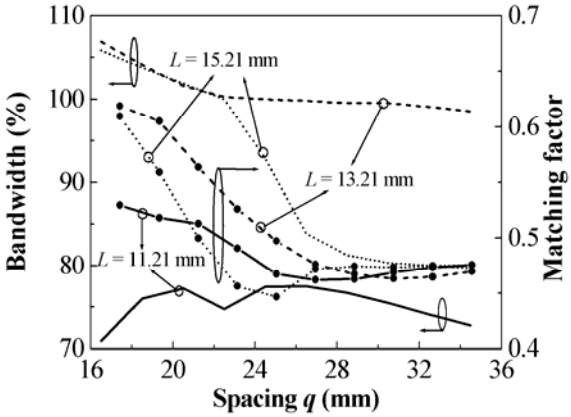

Fig. 10 Bandwidth and matching factor against the spacing q for varying stem lengths $L = l - v$

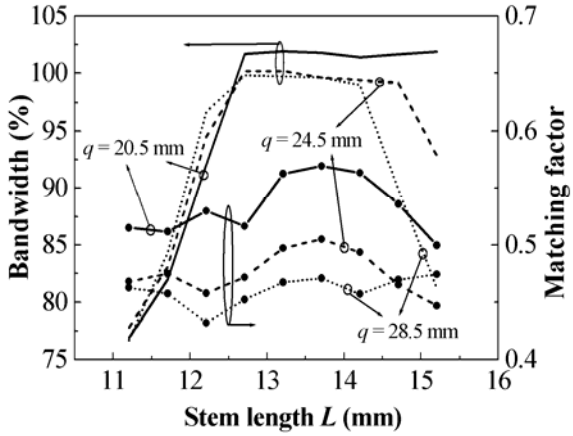

Fig. 11 Bandwidth and matching factor against the stem lengths $L = l - v$ for varying spacing q

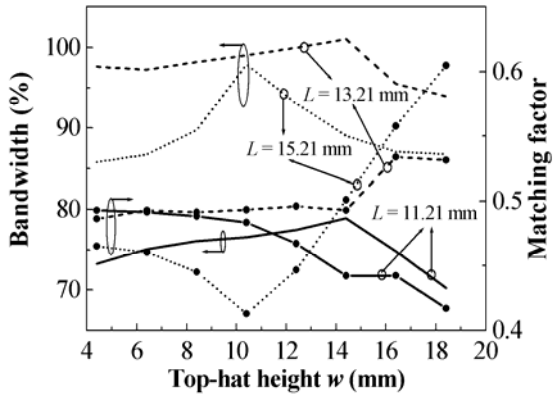

Fig. 12 Bandwidth and matching factor against the top-hat heights w for varying stem lengths $L = l - v$

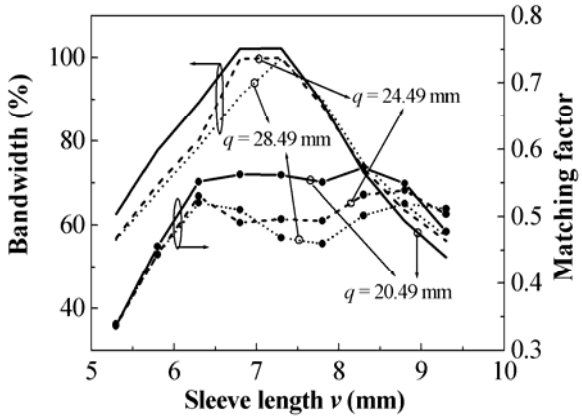

Fig. 13 Bandwidth and matching factor against the sleeve length v for varying spacing q

V. CONCLUSIONS

A top-hat sleeve UWB monopole antenna has been proposed and modeled by a model expansion technique. Its impedance and radiation characteristics have been investigated. The study has demonstrated that the introduction of a top hat and sleeves into a simple monopole allows the good impedance match and stable radiation patterns across a remarkably broad bandwidth of up to 105%, which can cover lower UWB band of 3.1-4.8 GHz very well. Due to its attractive impedance and radiation performance, the proposed monopole has promising applications in ultra-wideband/ broadband wireless communication and radar systems.

REFERENCES

[1] S. A. Schelkunoff, *Electromagnetic Waves*, Van Nostrand, New York, 1943

[2] G. H. Brown and O. M. Woodward, Jr., "Experimentally determined radiation characteristics of conical and triangular antennas," *RCA Rev.*, Vol.13, No.4, Dec. 1952, p.452

[3] C. H. Papas and R. W. P. King, "Radiation from wide-angle conical antennas fed by a coaxial line," *Proc. IRE*, Nov. 1949, p.1269

[4] C. E. Smith, C. M. Butler, and K. R. Umashankar, "Characteristics of a wire biconical antenna," *Microwave Journal*, Vol.22, Sept. 1979, pp.39-40

[5] G. H. Brown and O. M. Woodward, Jr., "Experimentally determined impedance characteristics of cylindrical antennas," *Proc. IRE*, Vol.33, 1945, pp.257-262

[6] A. G. Kandoian, "Three new antenna types and their applications," *Proc. IRE*, Vol.34, Feb. 1946, pp.70-75W

[7] S. Honda, M. Ito, H. Seki, and Y. Jinbo, "A disk monopole antenna with 1:8 impedance bandwidth and omnidirectional radiation pattern," *ISAP"92*, Sapporo, Japan, 1992, pp.1145-1148

[8] M. Hammoud, P. Poey, and F. Colombel, "Matching the input impedance of a broadband disc monopole," *Electronics Lett.*, Vol.29, No.4, 1993, pp.406-407

[9] M. J. Ammann, "Square Planar Monopole Antenna, "*IEE NCAP*, 1999, pp.37-40

[10] Z. N. Chen, "Impedance characteristics of planar bow-tie-like monopole antennas," *Electronics Lett.*, Vol.36, No.13, 2000, pp.1100-1101

[11] H. Nakano, N. Ikeda, Y. Wu, R. Suzuki, H. Mimaki, and J. Yamauchi, "Realization of dual-frequency and wide-band VSWR performances using normal-mode helical and inverted-F antennas," *IEEE Trans. Antennas Propagat.*, vol.46, June 1998, pp.788-793

[12] M. A. Morgan and F. K. Schwering, "Eigenmode analysis of dielectric loaded top-hat monopole antennas," *IEEE Trans. Antennas Propagat.*, vol. 42, pp. 54-61, Jan. 1994.

[13] R. W. P. King and T. T. Wu, "The cylindrical antenna with arbitrary driven point," *IEEE Trans.*

Antennas Propagat., vol.13, Sept. 1965, pp.710-718

[14] R. W. P. King "Asymmetrical driven antennas and sleeve dipole," *Proc. IRE*, vol.38, Oct. 1950, pp.1154-1164

[15] Z. N. Chen, K. Hirasawa, and K. Wu, "A broad-band sleeve monopole integrated into parallel-plate waveguide," *IEEE Trans. Microwave Theory Tech.*, vol. 48, July 2000, pp.1160-1163

[16] Z. N. Chen, K. Hirasawa, and K. Wu, "A novel top-sleeve monopole in two parallel plates," *IEEE Trans. Antennas Propagat.*, vol. 49 Mar. 2001, pp. 438-443

[17] M. A. Morgan, R. C. Hurley, and F. K. Schwering, "Computation of monopole antenna currents using cylindrical harmonics," *IEEE Trans. Antennas Propagat.*, vol. AP-38, July 1990, pp. 1130-1133

[18] Z. N. Chen, X. H. Wu, H. F. Li, N. Yang, and M. Y. W. Chia, "Considerations for source pulses and antennas in UWB radio systems," *IEEE Trans. Antennas Propagat.*, vol. 52, no.7, pp. 1739-1748, July 2004

[19] R. F. Harrington, *Time-Harmonic Electromagnetic Fields*, New York: McGraw-Hill, 1961